

PEDIATRIC HEAD AND NECK DYNAMICS IN FRONTAL IMPACT: ANALYSIS OF IMPORTANT MECHANICAL FACTORS AND PROPOSED NECK PERFORMANCE CORRIDORS FOR SIX AND TEN YEAR OLD ATDS

Alan T. Dobb
Hattie C. Cutcliffe
Jason F. Luck
Courtney A. Cox
Barry S. Myers
Cameron R. Bass
Roger W. Nightingale

Duke University, Department of Biomedical Engineering and Division of Orthopaedic Surgery
United States of America

Kristy B. Arbogast
Thomas Seacrist

Center for Injury Research and Prevention, Children's Hospital of Philadelphia
United States of America
Paper Number 13-0207

ABSTRACT

Traumatic injuries are the leading cause of death of children aged one to nineteen in the United States. These unintentional injuries are principally caused by motor vehicle collisions, with the head being the primary region injured. The neck, though not commonly injured, governs head kinematics and influences head impact location and velocity. Vehicle design improvements necessary to reduce or prevent these injuries are evaluated using anthropomorphic testing devices (ATDs). The head and neck properties of the current pediatric ATDs were established by scaling adult properties using the size differences between adults and children. Due to the paucity and limitations of pediatric head and neck biomechanical research, computational models are the only available methods that combine all existing biomechanical data to produce injury-relevant biofidelity specifications for pediatric ATDs. The purpose of this study is to provide the first frontal impact biofidelity corridors for neck flexion response of six and ten year olds using computational models incorporating pediatric cadaveric data. These corridors are compared with response of the Hybrid III (HIII) ATD necks and the Mertz flexion corridors.

Our six and ten year old head and neck multibody models used pediatric biomechanical properties obtained from pediatric cadaveric and radiological studies. The computations included the effect of passive and active musculature, and were validated with data including 3 g dynamic frontal impact responses using pediatric volunteer tests. Because ATD pendulum tests are used to calibrate HIII neck bending stiffness, we simulated these tests to

compare the pediatric model and HIII ATD neck bending stiffness, and to compare the model flexion bending responses with the Mertz scaled neck flexion corridors. Additionally, pediatric response corridors for both pendulum calibration tests and high speed (15 g) frontal impacts were estimated through uncertainty analyses on primary model variables. For the frontal impacts, adult boundary conditions and muscle activations, validated against 15 g volunteer tests, were applied to the pediatric models. Response corridors for each loading scenario were calculated from the average \pm standard deviation response over 650 simulations.

We found that the models were less stiff in dynamic anteroposterior bending than the pediatric ATDs, as the secant stiffness of the six and ten year old models was 53% and 67% less than that of the HIII ATDs. At higher rotation angles the ATDs exhibited nonlinear stiffening while the models demonstrated nonlinear softening. Consequently, the models did not remain within the Mertz scaled flexion bending corridors, especially for rotations above 60 degrees of flexion. The more compliant model necks suggest an increased potential for head impact via larger head excursions. In contrast with the Mertz corridors, no interactions between the head and chest were modeled in these simulations since the loading conditions used (pendulum calibration testing) do not include chin-on-chest contact. The pediatric anteroposterior bending corridors developed in this study are extensible to any frontal loading condition through calculation and sensitivity analysis. Our corridors are the first based on pediatric cadaveric data and provide the basis for future, more biofidelic designs of six and ten year old ATD necks.

INTRODUCTION

Traumatic injuries are the leading cause of death of children ages one to nineteen years in the United States (CDC 2007). The main source of these traumatic injuries is motor vehicle crashes (MVC), with the head being the primary body region injured (Durbin et al. 2001). The pediatric neck, although not commonly injured, governs head excursion and acceleration, thus influencing head impacts and injury during automobile collisions. Additionally, pediatric cervical spinal injuries are debilitating and often fatal. Of children sustaining these cervical injuries, the mortality rate was 27% and the overall incidence of neurological deficits was 66% (Platzer et al. 2007). While seating children in the rear seat of a vehicle in an age-specific restraint can decrease the likelihood of injury, additional pediatric MVC injuries can be prevented by design improvements to vehicle passenger compartments and restraint systems.

The principal tool used to evaluate these restraint systems and passenger compartment advances are anthropomorphic testing devices (ATD). While very useful, these child ATDs were developed with limited human pediatric biomechanical data. The head and neck dynamic response of the current pediatric ATDs are adult properties scaled using size differences between adults and children with limited incorporation of the material differences with age. The assessment of pediatric ATD biofidelity and injury criteria is limited by the paucity of pediatric head and neck biomechanical research. Common sources of this data include studies with human volunteers, cadavers, animal surrogates, and computer models. While valuable, each of these approaches has inherent limitations.

For instance, human volunteer studies are restricted to non-injurious loading scenarios. To date, only a single pediatric volunteer study at the Children's Hospital of Philadelphia (CHOP) has been published in which volunteers were subjected to frontal impact loading. During this study, adults and pediatric volunteers, aged six to fourteen years, were subjected to low-speed (<4 g) frontal impacts (Arbogast et al. 2009).

Moreover, cadaver studies are limited by the rare availability of pediatric cadavers, their lack of live-active musculature, and their inability to demonstrate minor injury, such as pain or loss of consciousness. Only a handful of pediatric cadaver studies of frontal impact tests have been conducted (Kallieris et al. 1976; Wismans et al. 1979; Dejeammes et al. 1984).

Though the pediatric cadavers in these studies were less stiff than their respective ATDs, the authors conclude that determining ATD performance criteria and injury values from their results would be speculative.

Animal surrogate studies provide valuable insights into the biomechanical response of the cervical spine. However, they are limited by interspecies differences in functional anatomy and the absence of scaling relationships from animal to human responses.

In view of the above limitations, computational modeling of the pediatric head and neck may prove to be the best method to provide biofidelity requirements and injury assessment reference values for child ATDs. Experimentally validated models incorporating accurate pediatric properties can simulate numerous loading conditions to investigate injury potential. While numerous models of the adult 50th percentile male have been created, a limited number of pediatric models exist (de Lange et al. 2001; Liu and Yang 2002; Mizuno et al. 2005; Dupuis et al. 2006; Meyer et al. 2009).

Accuracy of the computational model results is limited by the parameters—geometric and mechanical—upon which the model is founded. Thus, validation is critical to assess model biofidelity. Validation is the correlation of model responses to experimentally obtained result corridors, either cadaver or volunteer. Computer models of the head and neck have principally relied upon frontal impact simulations for validation, such as adult volunteer frontal impact experiments performed at the Naval Biodynamics Laboratory (NBDL) (Ewing and Thomas 1972; Wismans et al. 1986; Thunnissen et al. 1995).

To ensure repeatable and biofidelic response, dummies are also certified against such experimental or computational/scaled corridors. For example, the head and neck of the Hybrid III family of ATDs is certified before use in a frontal impact loading scenario (49 CFR 572, Subpart E). The ATD head and neck are attached to the end of a pendulum, which is raised and released. The pendulum arm is allowed to rotate under gravity until it impacts a block of aluminum (49 CFR 572, Subpart E). The pendulum deceleration results in head and neck flexion similar to a frontal impact. Computational models of the ATD head and neck have simulated this test for model validation (Doherty and Paver 1988; Yang and Le 1992; Marzougui et al. 1997; Medri et al. 2004). Similarly, models of the pediatric head and neck have used this test to validate against

scaled flexion corridors (de Lange et al. 2001; Mizuno et al. 2005; Dupuis et al. 2006).

The objective of this study was to use validated pediatric head and neck computer models that incorporate biomechanical properties from pediatric volunteer and cadaver studies to provide frontal impact biofidelity corridors for pediatric ATDS. Specifically, neck dynamic bending corridors were developed using a statistical uncertainty analysis for six and ten year olds based on the dynamic bending stiffness response of validated pediatric computational models for the pendulum certification test and for 15 g frontal impacts. These corridors were compared to that of the adult, the Hybrid III pediatric ATDs, and the Irwin and Mertz (1997) scaled neck flexion corridor.

METHODS

Model Development

The adult 50th percentile male computational head and neck model developed and used in the current study is a hybrid multibody and finite element model (Dibb 2011), as shown in Figure 1. Previous models (Camacho 1998; Van Ee 2000; Chancey 2005) provided the foundation for the current model (Dibb 2011). The osteoligamentous cervical spine was modeled with rigid body vertebrae connected by six degree of freedom non-linear viscoelastic beam intervertebral joints. A viscoelastic finite element head was implemented for head impact studies but was modeled as a rigid body for the purpose of this study. The material and inertial properties for the head, vertebrae, and muscles were developed from literature. Cervical musculature was modeled using Hill-type discrete beams. Muscle models were rate sensitive and included passive and active musculature (Hill 1938). Muscle wrapping was implemented to account for the interactions between individual muscles and vertebrae during bending (Dibb et al. 2013). Modeling and analysis were performed using LS-DYNA (LSTC, Livermore, CA). This adult model was validated in low-speed (<4 g) frontal impacts (Dibb et al. 2013), using data from CHOP (Arbogast et al. 2009), and in 15 g frontal impacts, using from NBDL (Ewing and Thomas 1972).

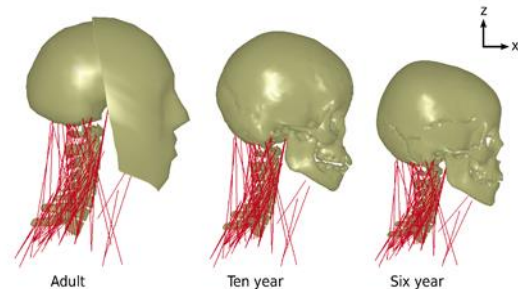


Figure 1. Lateral view of the adult and pediatric head and neck models.

The pediatric head and neck models of the current study (Figure 1) represent a 50th percentile six and ten year old and were created upon the same framework as the adult model, while incorporating pediatric biomechanical properties from pediatric volunteer and cadaver studies. The pediatric head models were developed using pediatric geometric and inertial properties reported by Loyd et al. (2010), while cervical vertebral geometric and inertial properties were developed from pediatric volunteer and cadaver radiology studies, respectively (Dibb 2011). Likewise, cervical muscle cross-sectional areas and attachment locations were developed from human pediatric and adult radiology studies (Dibb 2011). Intervertebral joint stiffnesses were derived from pediatric cadaver osteoligamentous cervical spine mechanical tests (Luck et al. 2008; Luck et al. 2012). These pediatric head and neck models were validated in frontal impacts (Dibb et al. 2013) using the only pediatric head and neck biofidelity validation currently available: the CHOP low-speed (<4 g) human volunteer tests (Arbogast et al. 2009).

Pendulum Certification Simulation

Simulations of the ATD neck pendulum calibration test with the adult and pediatric models were performed to compare the neck sagittal dynamic bending stiffness between the pediatric models and: the adult model, the pediatric Hybrid III ATD necks, and the Irwin and Mertz (1997) scaled neck flexion corridor. In these simulations, the pendulum was modeled as a rigid solid with physical and inertial dimensions as detailed in the Hybrid III 50th percentile male ATD test procedure (49 CFR 572, Subpart E). It was constrained to rotate about the y-axis only. The T1 vertebrae of the head and neck models were rigidly attached to the end of the pendulum such that the radial distance between the pivot and head CG was equivalent for the ATD and adult model. The pendulum with attached head and neck model was initiated in the vertical position, as specified in the certification test (49 CFR 572,

Subpart E), with the specified rotational velocity. Each model was ran with the appropriate pendulum impact velocity, according to the model's age: 7.01 m/s as specified by the Hybrid III (HIII) 50th percentile male ATD (49 CFR 572, Subpart E) certification test procedure, 4.95 m/s as specified by the HIII six year old ATD (49 CFR 572, Subpart N) test procedure, or 6.10 m/s as specified by the HIII ten year old ATD (49 CFR 572, Subpart T) test procedure (Figure 2). Additionally, the adult and 10 year old models were ran at the HIII six year old certification velocity of 4.95 m/s for comparison between model responses. Decelerations were defined at the specified accelerometer attachment radius for both impact velocities.

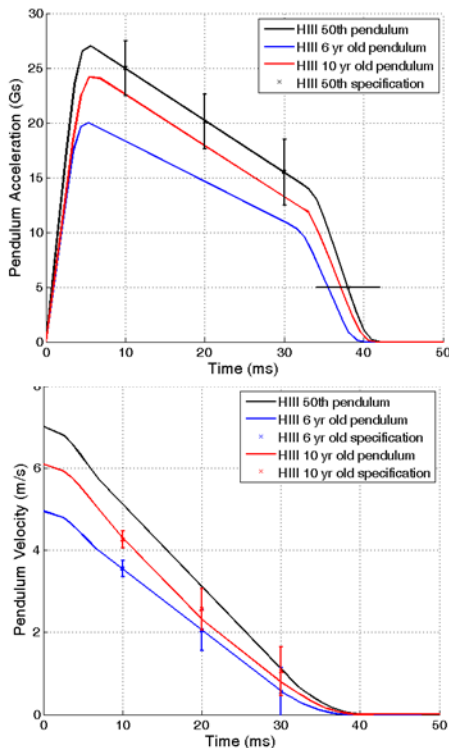


Figure 2. Applied pendulum deceleration and subsequent velocity time histories with the Hybrid III 50th percentile male, six year old ATD, and ten year old ATD certification specifications. The adult Hybrid III 50th percentile male standard specifies an acceleration corridor while the Hybrid III six and ten year old standards specify a velocity corridor. The corresponding pediatric acceleration and adult velocity profiles are plotted for comparison.

Biofidelity corridors for the pendulum certification tests were created from uncertainty analyses of the pediatric models with their corresponding pendulum velocity by varying the thirteen pediatric model input

parameters \pm one standard deviation (Table 1). These input values were scale factors developed from the ratio of the measured child to measured adult values for each parameter. For example, the adult model neck length, defined as the distance between the occipital condyle-C1 joint center of rotation and the C7-T1 joint center of rotation, was 14.08 cm. The ten and six year old model neck lengths were 12.35 and 9.80 cm, respectively. Input parameter values were selected using Latin hypercube sampling and 50 simulations were run per variable (Iman et al. 1981a; Iman et al. 1981b), for a total of 650 simulations. Correlation of stiffness to input variable was quantified through Pearson correlation with significance levels of $p < 0.05$. Model uncertainty corridors were created from the average \pm one standard deviation over all simulations.

Muscle activations were initially set to a relaxed activation state (Dibb et al. 2013), since pediatric motor vehicle occupants are likely not aware of impending impacts. However, the dynamics result in muscle activations due to stretch mediated activation, so the extensor muscles as a group were activated to 100% at the pendulum impact, with no delay time. Muscle activation dynamics were modeled using Hill-type muscle models and two first-order systems (Hill 1938; Winters and Stark 1985; Winters and Stark 1988), and 100% was chosen to bracket the response. A delay time was not incorporated for the pendulum certification test. Similarly, chin-on-chest contact was not modeled in these simulations as this contact is not accounted for in the pendulum certification test, and thus peak head excursions in the simulation were unimpeded. Gravity was modeled in the inferior to superior direction to simulate an inverted posture, and simulations were run for 200 ms.

The model head rotation was measured relative to the pendulum longitudinal centerline. The model sagittal moment at the occipital condyle (OC) joint was calculated from the ligamentous joint and the sum of all the muscle moments about the O-C2 joint center of rotation (COR). Therefore, the OC moment reported in this study is the total neck moment (sum of the ligamentous loads and all muscle moments about the O-C2 joint COR), not the moment seen by the OC joint alone. Secant stiffness was calculated at peak OC moment, as the slope of the line between zero and peak on a plot of OC moment versus head rotation.

Table 1. Pediatric Head and Neck Uncertainty Analysis Parameters (average \pm one standard deviation; each value given is a ratio of the pediatric to adult* value and thus is unitless)

Parameter	Age		Pediatric Value Reference
	Six Years	Ten Years	
Head mass	0.75 \pm 0.02	0.80 \pm 0.02	Loyd et al. 2010
Head inertia	0.58 \pm 0.09	0.62 \pm 0.10	Loyd et al. 2010
Head size x	0.92 \pm 0.03	0.93 \pm 0.03	Loyd et al. 2010
Head size y	0.92 \pm 0.03	0.93 \pm 0.03	Loyd et al. 2010
Head size z	0.74 \pm 0.06	0.77 \pm 0.06	Loyd et al. 2010
Vertebra mass	0.47 \pm 0.07	0.62 \pm 0.07	Dibb 2011
Vertebra inertia y	0.26 \pm 0.05	0.44 \pm 0.05	Dibb 2011
Vertebra size x	0.73 \pm 0.08	0.80 \pm 0.08	Dibb 2011
Vertebra size y	0.82 \pm 0.06	0.85 \pm 0.06	Dibb 2011
Vertebra size z	0.70 \pm 0.09	0.88 \pm 0.11	Dibb 2011
Intervertebral joint stiffness (Upper cervical spine)	0.44 \pm 0.11	0.58 \pm 0.09	Luck et al. 2008, Luck et al. 2012
Intervertebral joint stiffness (Lower cervical spine)	0.75 \pm 0.12	0.88 \pm 0.13	Luck et al. 2008, Luck et al. 2012
Muscle PCSA	0.47 \pm 0.09	0.57 \pm 0.12	Dibb 2011

*Adult values, previously cited during development of the Duke Adult Head and Neck Model, can be reviewed in Dibb 2011, Chancey 2005, Van Ee 2000, and Camacho 1998

NBDL 15 g Frontal Impact Simulation

The adult and pediatric head and neck models were subjected to 15 g frontal impact loading (Figure 3). To simulate this loading, the average T1 x-direction accelerations and y-direction rotational displacements from the NBDL volunteer tests (Ewing and Thomas 1972; Thunnissen et al. 1995) were applied to the T1 vertebra of the models (Figure 3). The same adult volunteer NBDL T1 boundary conditions were applied to the pediatric models (Figure 3) as well as the same muscle activation dynamics (Figure 4) (Dibb 2011). Muscle activation dynamics were modeled using Hill-type muscle models and two first-order systems (Hill 1938; Winters and Stark 1985; Winters and Stark 1988). The simulations were initiated with relaxed muscle activation states that maintained an upright posture against gravity (Dibb 2011; e.g. Dibb et al. 2013). Extensor muscles were then activated to 100% (Figure 4), again chosen to bracket the response, after a reflex delay time. As muscle reflex delay times range in the literature from 10 to 120 ms (Colebatch et al. 1994; Foust et al. 1973; Reid et al. 1981; Schneider et al. 1975; Tennyson et al. 1977; Siegmund et al. 2003), a time of 50 ms was used in this simulation. Gravity was simulated as a constant body load in the superior to inferior direction.

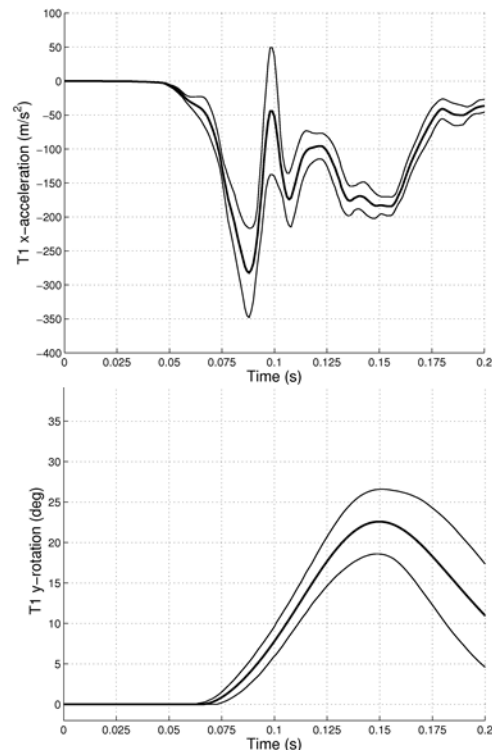


Figure 3. Imposed T1 horizontal acceleration and sagittal rotation time history from 15 g NBDL human male volunteer frontal impact tests, average \pm one standard deviation (adapted from Thunnissen et al. 1995). The average histories were applied in all of our simulation.

Biofidelity response corridors were developed through uncertainty analyses of the adult and pediatric models, since pediatric volunteer high speed frontal impact experiments cannot be conducted due to the possibility of serious injury. The thirteen pediatric model input parameters were varied plus and minus one standard deviation (Table 1). Input parameter values were selected using Latin hypercube sampling and 50 simulations were run per variable (Iman et al. 1981a; Iman et al. 1981b), for a total of 650 simulations. The dependence of peak model responses and OC neck loads on input variables were quantified through Pearson correlation with significance levels of $p < 0.05$. Pediatric model response corridors were created from the average \pm one standard deviation over all simulations.

Adult model kinematic and kinetic responses were validated against the NBDL volunteer response corridors (Dibb 2011) defined as the average response plus and minus the standard deviation (Thunnissen et al. 1995). Accelerations were defined relative to the global coordinate system while displacements were defined relative to a local coordinate system fixed to the midsagittal anterior-superior corner of the T1 vertebral body. Head accelerations and displacements were defined at the head CG. Neck rotations were defined as the rotation of a linkage that connected the T1 local coordinate origin to the OC center of rotation. Neck loads were calculated at the vertebral joints, including the OC, by summing the ligamentous and the muscular contribution about the vertebral joint COR. Neck loads were relative to the head anatomical coordinate system. The secant head and neck bending stiffness was calculated from the head rotation and OC joint neck moment.

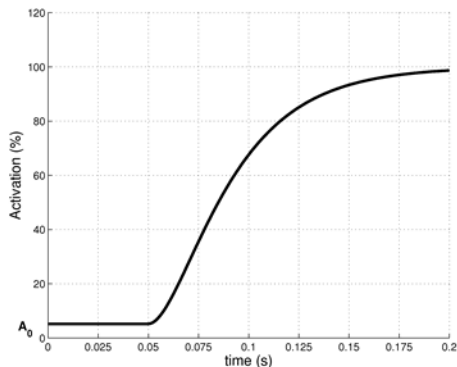


Figure 4. Activation dynamic time history of the extensors during 15 g frontal impact, modeled using Hill-type muscle models and two first-order systems. Initial activations, A_0 , maintained an upright head posture against gravity. Activations were then increased to 100% after a reflex time ($t = 50$ ms).

RESULTS

Pendulum Certification Simulation

The response of the pediatric six and ten year old models during pendulum induced frontal impact with the HIII six year old certification velocity (49 CFR 527, Subpart N) was similar to the adult response at the same velocity (Figures 5 and 6). The adult 50th percentile male model first went into extension rotation, followed quickly by flexion rotation upon impact (Figure 6). Extension peaked at -4° head rotation. Peak head flexion of 111° occurred 97 ms after impact, while peak flexion moment of 51.2 Nm occurred earlier, at 85 ms after impact. The flexion moment reached 90% of its peak magnitude by 55 ms and increased the final 10% during the next 27 ms. OC moment decreased by 17% at the time of peak head rotation. The pediatric model heads also initially extended, reaching a peak of -3° head rotation. The head of the pediatric models then rotated into flexion with greater rotational displacements and lower OC flexion moments than the adult model, indicating that the pediatric necks were less stiff than the adult.

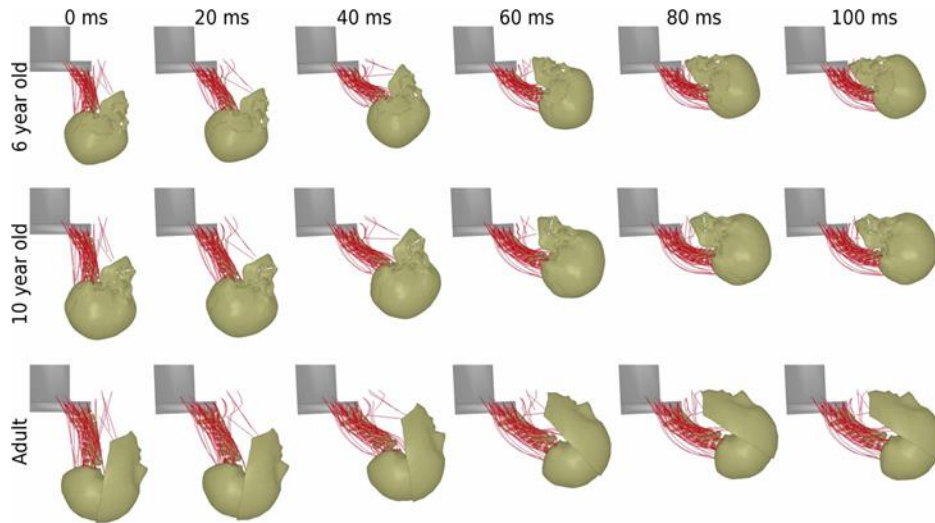


Figure 5. Adult and pediatric kinematic time-lapse during the six year old pendulum certification test. The pediatric models had larger peak head rotations than the adult.

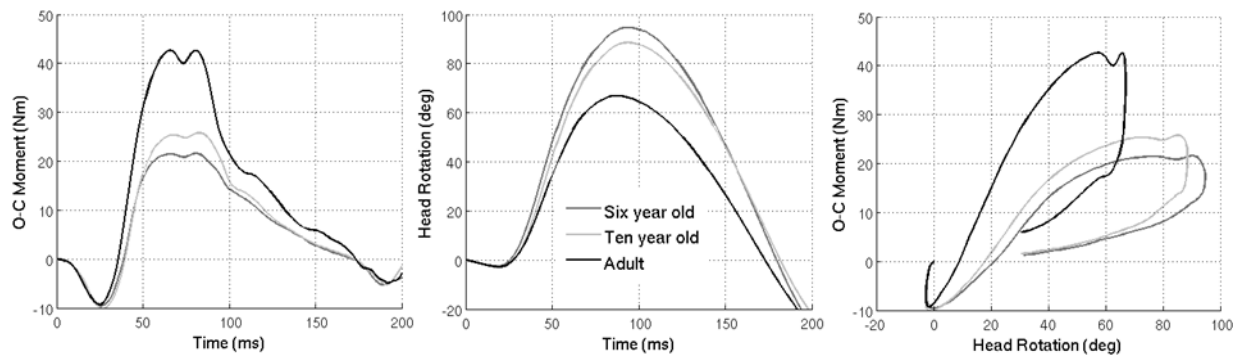


Figure 6. Pediatric and adult model head rotation and OC moment during the six year old pendulum certification test. The pediatric models are more compliant than the adult, as indicated by the slope of the loading curve. Both the pediatric and adult models rotated first into extension before rotating into flexion.

Pediatric model uncertainty analysis corridors are presented in Figure 7. The six year old average peak OC moment was 22 ± 1.7 Nm at 85 ± 10 degrees of head flexion. The ten year old average peak OC moment was 28 ± 2.1 Nm at 110 ± 14.6 degrees of head flexion. The average secant stiffness during the uncertainty analysis was 0.27 ± 0.05 Nm/deg for both the six and ten year old models, respectively. Pediatric model bending stiffnesses were most sensitive to muscle physiological cross-sectional area (PCSA). Increasing the muscle PCSA significantly increased the bending stiffness, as this increased the force-generating capacity of the muscles. Bending stiffness correlation coefficients to pediatric model parameters are presented in Table 2. The next most significant parameters were vertebral and head geometry scale factors in the x and z directions, which altered muscle attachment locations and thus their effective moment arms. Increasing these factors also increased the bending stiffness of the models.

Increasing the osteoligamentous bending stiffness increased the neck bending stiffness too; however, the muscle parameters and geometric scale factors mentioned previously had greater effects.

The pediatric models with muscle tension were less stiff than the Hybrid III six year old (NHTSA 1998; Saul et al. 1998) and ten year old ATD (Mertz et al. 2001), as shown in Figure 8. The secant stiffness of the six year old model was 0.24 Nm/deg and of the ten year old was 0.25 Nm/deg. This was 53% and 67% less than the HIII six and ten year old ATD stiffnesses of 0.50 and 0.75 Nm/deg, respectively. In addition, the qualitative response of the model and the Hybrid III were different; the pediatric model flexion bending stiffnesses were nonlinear softening while the HIII were nonlinear stiffening. Due to these differences in nonlinearity, the pediatric models did not remain within the Irwin and Mertz (1997) scaled flexion bending corridors (Figure 8).

Table 2. Pediatric Model Bending Stiffness Pearson Correlation Coefficients During Pendulum Uncertainty Analysis (* indicates statistically significant; the three most important parameters for each model are in bold)

Parameter	Stiffness Correlation	
	Six Years	Ten Years
Vertebra geometry – x	0.18*	0.11*
Vertebra geometry – y	-0.03	-0.07
Vertebra geometry – z	-0.16*	-0.16*
Vertebra mass	0.07	0.07
Vertebra inertia	0.02	0.02
Head geometry – x	0.09	0.12*
Head geometry – y	0.00	-0.01
Head geometry – z	-0.18*	-0.10
Head mass	-0.07	-0.04
Head inertia	0.09	0.05
Intervertebral joint stiffness (Upper cervical spine)	-0.14*	-0.04
Intervertebral joint stiffness (Lower cervical spine)	-0.01	-0.01
Muscle PCSA	0.88*	0.88*

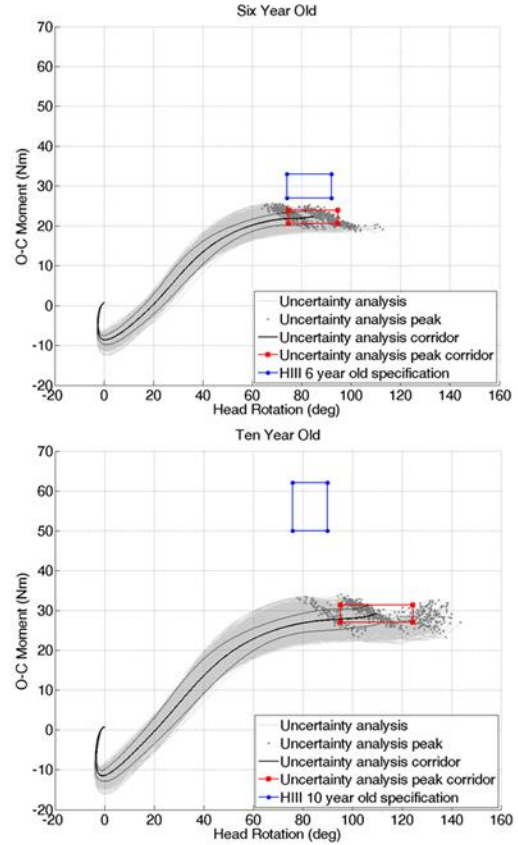


Figure 7. Pediatric model flexion stiffness uncertainty analysis corridors for pendulum certification tests. Plotted are all 650 simulations with response corridors created from the average \pm standard deviation. Model stiffness for both pediatric models was most sensitive to muscle PCSA.

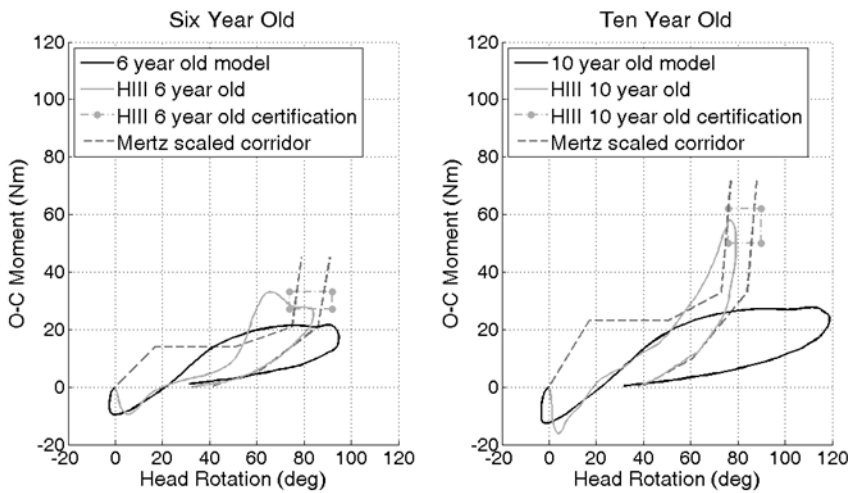


Figure 8. The pediatric head and neck models demonstrated qualitatively different behavior than the Hybrid III six and ten year old ATD in pendulum certification tests. The models were less stiff than the Hybrid III ATDs and their behavior was not predicted by the Irwin and Mertz (1997) scaled flexion corridor.

NBDL 15 g Frontal Impact Simulation

The response of the pediatric six and ten year old head and neck models to 15 g frontal impact was similar to the adult model response (Figure 9), which reproduced the kinematic response of adult human volunteers to 15 g frontal impact (Dibb 2011). During

the first 80 ms there was little head motion and the relaxed state muscles maintained an upright posture against gravity. From 80 to 106 ms, the head began to translate but did not begin to rotate. This 26 ms delay in head rotation is termed head lag. Afterwards, the head rotated into flexion. After reaching peak angular displacement, the head started rebounding.

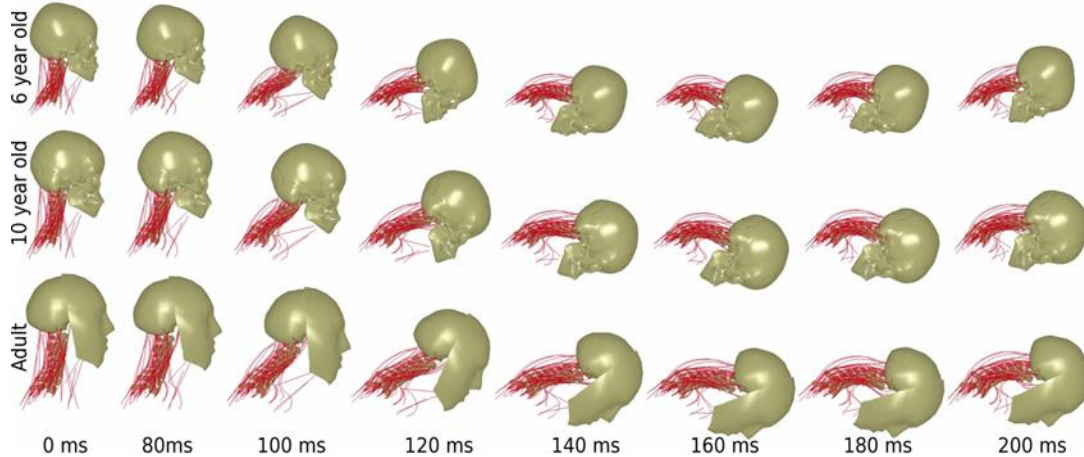


Figure 9. Pediatric and adult model response time-lapse in 15 g frontal impact. The pediatric models had larger peak head rotations than the adult.

As in the pendulum certification tests, the pediatric models had smaller head excursions but greater rotations than the adult (Table 3 and Figure 10). Specifically, the six and ten year old models displaced 30% and 14% less in the x-direction and 21% and 5% less in the z-direction. This is not unexpected given the shorter overall lengths of the pediatric necks. The head of both the six and ten year old models rotated 11% more than the adult. This is not unexpected, since rotation is dependent on the head mass and moment of inertia (MOI). The ratio of head MOI to head mass is very similar for the six and ten year old models, leading to a very similar amount of rotation. On the other hand, the adult ratio of head MOI to head mass is less than that of the pediatric models, and consequently demonstrates less rotation.

Table 3. Pediatric and Adult Model Peak Responses During 15 g Frontal Impact

Response	Six Years	Ten Years	Adult
Head displacement x	10.1 cm	12.5 cm	14.5 cm
Head displacement z	12.2 cm	14.6 cm	15.4 cm
Head rotation	76.1 deg	76.2 deg	68.4 deg
Head acceleration x	286 m/s ²	258 m/s ²	243 m/s ²
Head acceleration z	174m/s ²	185 m/s ²	172 m/s ²
Head rot. acceleration	2571 rad/s ²	2208 rad/s ²	1534 rad/s ²
Neck rotation	65.6 deg	67.9 deg	62.5 deg
Head lag	26 ms	26 ms	26 ms

The pediatric models had greater head translational and rotational accelerations than the adult (Table 3 and Figure 10). Head x-direction translational accelerations for the six and ten year old models were 17% and 6% greater than the adult, respectively. Head sagittal rotational accelerations for the six and ten year old model were 68% and 44% greater than the adult, respectively. These higher accelerations resulted in earlier peak excursions and rotations, and the six and ten year old models reached peak head rotation 19 and 11 ms earlier than the adult.

Furthermore, the pediatric models sustained lower cross-sectional neck flexion moment and tensile loads than the adult (Figure 11). The total cross-sectional peak flexion moment at the OC was only 20.9 and 25.5 Nm in the six and ten year old models compared to 46.5 Nm in the adult. The total cross-sectional peak tensile force at the OC was 648 and 713 N in the six and ten year old models compared to 859 N in the adult. On the other hand, the pediatric models sustained higher peak shear loads than the

adult model. The total cross-sectional peak shear force at the OC was 950 and 861 N for the six and ten year old models compared to 835 N for the adult.

In all models, the neck muscles were the primary moment and force-carrying component of the total

neck during 15 g frontal impacts (Figure 11). As illustrated by comparing the ligamentous, muscular, and total F_z neck loads, the osteoligamentous spine was loaded in compression during peak neck flexion at the same time the total neck was loaded in tension.

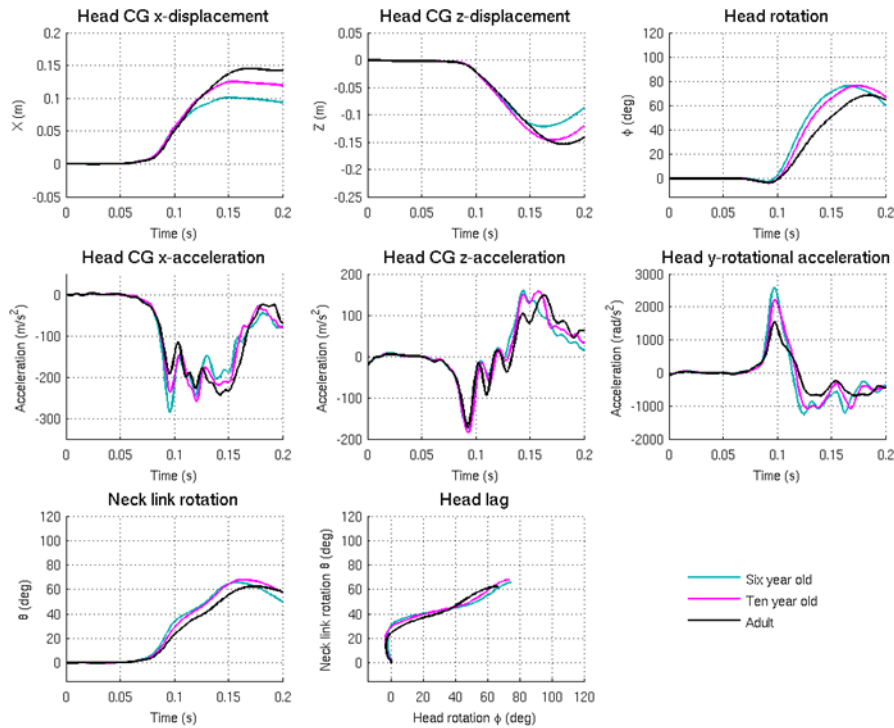


Figure 10. Pediatric and adult model kinematic response to 15 g frontal impact. The heads of the six and ten year old models displaced less but rotated more than the adult.

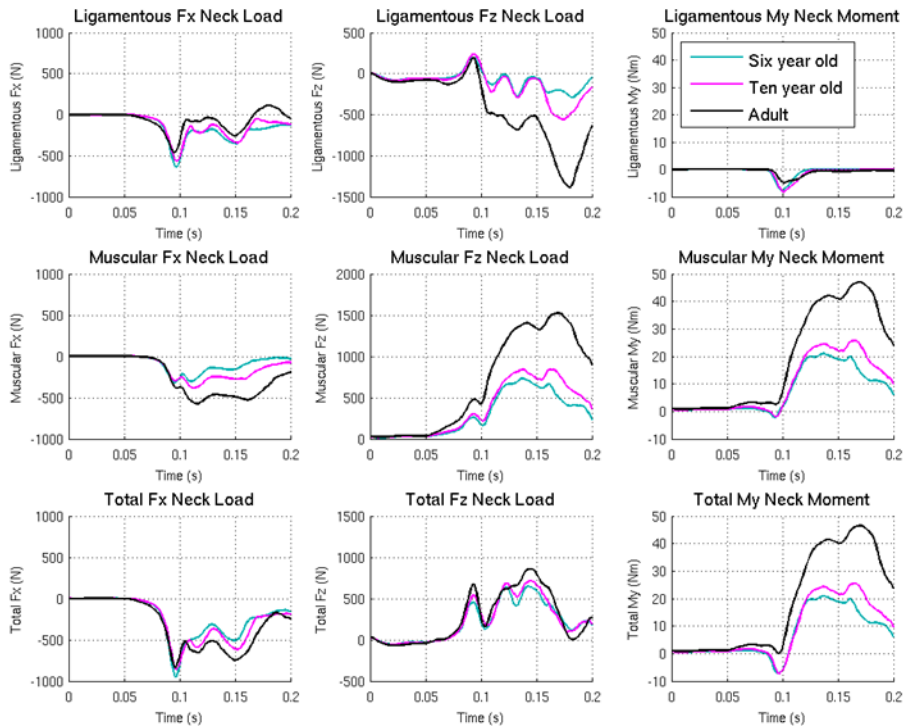


Figure 11. Pediatric and adult model O-C2 spinal segment osteoligamentous, muscular, and total neck loads during 15 g frontal impact. The cervical muscles bore a majority of the loading during this impact. At peak neck flexion, the osteoligamentous spine was loaded in compression while the total neck was loaded in tension.

From the uncertainty analysis, the kinematic response of the pediatric models was most sensitive to the z-direction vertebral geometry scale factor. Correlation coefficients of model parameters to kinematic responses are presented in Table 4. Increasing the z-direction scale factor—which in turn increased the length of the pediatric neck—significantly increased peak head displacements, head rotation, and z-direction translational accelerations; increasing this value also significantly decreased the peak x-direction translational acceleration and head rotational acceleration.

The next most significant parameters affecting the kinematic response were muscle PCSA and the z-direction head geometry scale factors. Increasing these scale factors increased the muscle size and the muscle attachment distance from the spine, or moment arm. Increases in these parameters significantly decreased peak head flexion rotation and decreased head rotational accelerations. Increasing the intervertebral joint stiffness did not significantly affect peak head excursion or rotations; however, increasing the joint stiffnesses did increase peak head accelerations. Additionally, cross-sectional neck loads measured at the OC spinal segment were most sensitive to pediatric muscle PCSA, vertebral and head z-direction geometry, and head inertial property scale factors (Table 5). As before,

intervertebral joint stiffnesses only significantly affected peak OC tensile forces.

Six and ten year old pediatric response corridors during 15 g frontal impact are presented in Figures 12 and 13.

Table 4. Pediatric Model Uncertainty Analyses Kinematic Pearson Correlation Coefficients During 15 g Frontal Impact, Presented and Ranked Against Other Model Parameters
 (* indicates statistically significant; the top three parameters in each column of each age are in bold)

	Parameter	Peak CG displacement x	Peak CG displacement z	Peak head rot.	Peak CG accel. x	Peak CG accel. z	Peak head rot. accel.	Peak neck rot.	Head lag time
Six Years	Vertebra geometry - x	-0.08	-0.22*	-0.24*	-0.02	-0.45*	-0.07	-0.43*	-0.33*
	Vertebra geometry - y	0.04	0.07	0.05	0.00	0.04	0.04	0.09	0.13*
	Vertebra geometry - z	0.94*	0.76*	0.37*	-0.73*	0.69*	-0.41*	0.63*	0.59*
	Vertebra mass	0.01	-0.01	-0.04	-0.04	-0.01	-0.04	0.01	0.03
	Vertebra inertia	0.00	-0.01	0.00	0.01	-0.01	-0.06	-0.04	0.02
	Head geometry - x	-0.08	-0.06	-0.14*	0.07	-0.05	0.00	0.01	-0.01
	Head geometry - y	0.05	0.03	0.01	-0.08	0.04	-0.01	0.00	-0.05
	Head geometry - z	0.28*	0.25*	0.23*	-0.33*	-0.13*	-0.06	0.08	-0.34*
	Head mass	0.00	0.10	0.13*	0.04	0.07	0.18*	0.17*	0.01
	Head inertia	-0.02	0.04	0.14*	0.24*	-0.28*	-0.53*	-0.08	0.47*
	Joint stiffness - upper cerv. spine	0.01	0.02	0.01	0.05	0.08	0.20*	0.03	-0.14*
	Joint stiffness - lower cerv. spine	0.01	-0.09	-0.03	0.04	0.33*	0.08	-0.28*	-0.09
	Muscle PCSA	-0.07	-0.55*	-0.85*	-0.43*	-0.21*	-0.65*	-0.54*	-0.08
Ten Years	Vertebra geometry - x	-0.07	-0.19*	-0.19*	-0.39*	-0.52*	-0.10	-0.36*	-0.19*
	Vertebra geometry - y	0.05	0.06	0.05	0.05	0.07	0.03	0.08	0.10
	Vertebra geometry - z	0.96*	0.78*	0.43*	-0.41*	0.73*	-0.45*	0.66*	0.71*
	Vertebra mass	0.01	-0.01	-0.04	-0.01	0.01	-0.03	0.00	0.04
	Vertebra inertia	0.00	0.00	0.01	-0.01	-0.01	-0.06	-0.03	0.01
	Head geometry - x	-0.09	-0.06	-0.12*	-0.07	-0.03	0.01	-0.02	-0.04
	Head geometry - y	0.05	0.02	0.01	0.07	0.02	-0.01	0.01	-0.03
	Head geometry - z	0.23*	0.21*	0.24*	0.27*	-0.18*	-0.08	0.06	-0.29*
	Head mass	0.01	0.09	0.11	-0.08	0.04	0.16*	0.15*	-0.03
	Head inertia	-0.01	0.05	0.12*	-0.25*	-0.11	-0.51*	-0.03	0.47*
	Joint stiffness - upper cerv. spine	0.01	0.01	0.01	0.28*	-0.05	0.12*	0.02	-0.10
	Joint stiffness - lower cerv. spine	0.02	-0.06	-0.01	0.25*	0.30*	0.04	-0.19*	-0.04
	Muscle PCSA	-0.13*	-0.57*	-0.85*	-0.04	-0.28*	-0.65*	-0.62*	-0.07

Table 5. Pediatric Model Uncertainty Analyses Kinetic Pearson Correlation Coefficients During 15 g Frontal Impact, Presented and Ranked Against Other Model Parameters
 (* indicates statistically significant; the top three parameters in each column of each age are in bold)

	Parameter	Peak OC Shear Force	Peak OC Tensile Force	Peak OC Flexion Moment
Six Years	Vertebra geometry - x	0.02	-0.07	0.10
	Vertebra geometry - y	0.00	-0.05	-0.04
	Vertebra geometry - z	0.48*	0.01	-0.15*
	Vertebra mass	0.02	-0.04	0.05
	Vertebra inertia	-0.02	0.03	0.01
	Head geometry - x	-0.05	-0.28*	0.08
	Head geometry - y	0.07	0.07	0.01
	Head geometry - z	0.40*	0.53*	0.12*
	Head mass	-0.37*	0.30*	-0.03
	Head inertia	-0.26*	0.35*	0.15*
	Intervertebral joint stiffness – upper cervical spine	0.01	0.31*	-0.02
	Intervertebral joint stiffness – lower cervical spine	-0.06	0.21*	0.06
	Muscle PCSA	0.58*	-0.25*	0.95*
Ten Years	Vertebra geometry - x	0.03	-0.21*	-0.01
	Vertebra geometry - y	-0.01	-0.01	-0.04
	Vertebra geometry - z	0.60*	0.20*	-0.04
	Vertebra mass	0.02	-0.04	0.04
	Vertebra inertia	-0.01	0.02	0.01
	Head geometry - x	-0.09	-0.20*	0.11
	Head geometry - y	0.07	0.06	0.03
	Head geometry - z	0.33*	0.56*	0.28*
	Head mass	-0.31*	0.28*	-0.02
	Head inertia	-0.21*	0.10	0.05
	Intervertebral joint stiffness – upper cervical spine	0.02	0.20*	0.03
	Intervertebral joint stiffness – lower cervical spine	0.01	0.13*	0.06
	Muscle PCSA	0.57*	-0.49*	0.93*

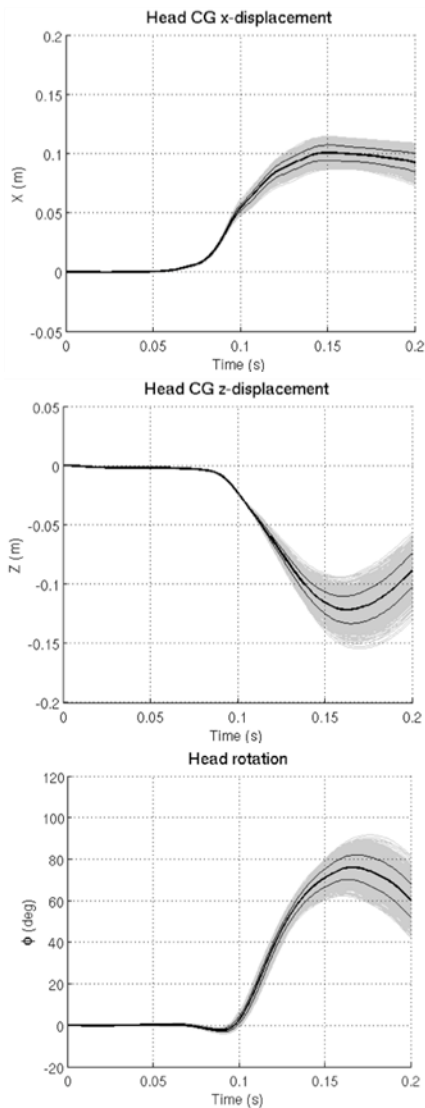


Figure 12. Six year old model head CG translational and rotational responses during 15 g frontal impact uncertainty analysis. Plotted are all 650 simulations with the corridor created from the average \pm standard deviation.

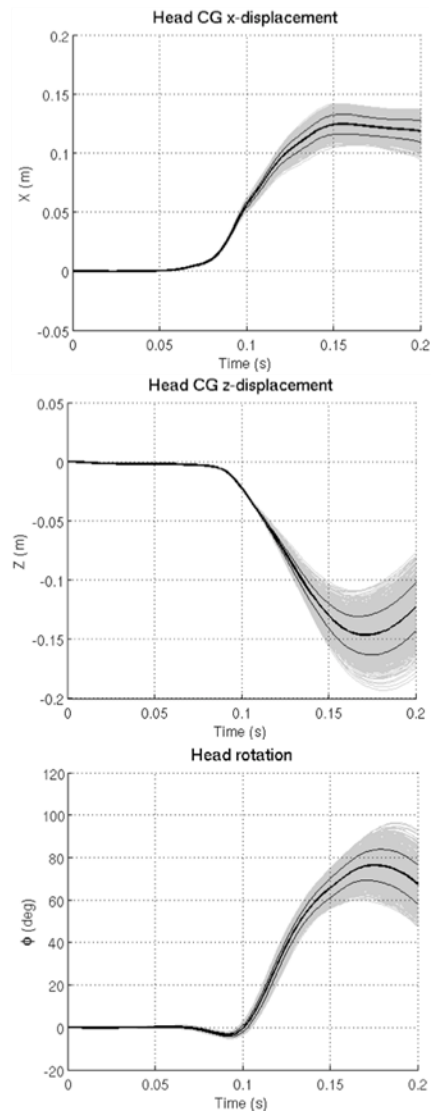


Figure 13. Ten year old model head CG translational and rotational responses during 15 g frontal impact uncertainty analysis. Plotted are all 650 simulations with the corridor created from the average \pm standard deviation.

DISCUSSION

The purpose of this study was to utilize a pediatric head and neck multibody and finite element model to investigate the head kinematics and dynamic flexion bending response and stiffness of the neck during ATD neck certification pendulum testing. Also created and studied were flexion biofidelity corridors for future pediatric ATD design for both pendulum certification tests and 15 G frontal impacts.

In the pendulum certification tests, the pediatric neck was less stiff than the adult neck. Likewise, the pediatric necks were less stiff in flexion bending than the Hybrid III ATD necks: the six year old was 53% less stiff than the ATD while the ten year old was 67% less stiff. The difference between ATD and model bending stiffness was minimal below 40° of head flexion, while greater differences occurred at higher rotations. At higher rotations the ATD stiffness nonlinearly increased while the model stiffness nonlinearly decreased. The muscles and their strain rate dependence can explain this nonlinear softening of the models. Muscle force increases at higher elongation strain rates in both the passive and active elements (Hill 1938; Myers et al. 1998; Winters 1990; Winters 1995). Since higher muscle strain rates occurred during the higher head rotational velocities of the initial loading phase, and then decreased until peak head rotational displacement was reached, the muscle force decreased as peak head rotational displacements were reached. This is illustrated by the OC moment time histories (Figure 6). The moments increased rapidly during the high muscle strain rate of the initial loading and peaked prior to peak rotational displacement, then decreased by peak rotation. A secondary explanation of the softening of model bending stiffness is the decrease in stress of the active muscle with increased strains (Hill 1938; Myers et al. 1998; Winters 1990; Winters 1995). However, the active muscle strain dependence was less of a factor since muscle strains were relatively low with an average peak extensor strain of only 11%. Therefore, an important difference in stiffness between the models and the Hybrid III ATD necks is the strain rate dependent effects that are not accounted for in the design of the ATD necks.

In a similar fashion, the pediatric and adult model flexion bending response all passed outside of the Mertz corridors, primarily at higher head rotations. This is because the model bending stiffness did not increase at higher rotations, and instead decreased. This behavior was consistent for both the six and the ten year old, and illustrates that the Mertz corridors

predict qualitatively different behavior than the neck models display.

Though chin-on-chest contact was not modeled in these simulations, the pendulum flexion bending biofidelity response corridors created from uncertainty analysis of the models' response (Figure 7) are appropriate since this contact is not accounted for in the Hybrid III pendulum certification test. Therefore, these corridors represent the response of validated, biofidelic models under the same loading conditions used to certify the ATD neck, and can be used for future pediatric ATD neck design specification. Importantly, both the head extension, which occurs prior to flexion, and the nonlinear softening behavior were included in the corridors. Neither of these effects is represented by the current Hybrid III ATD necks. Muscle parameters had the greatest effect on neck bending stiffness. Increasing the force generating capacity, effective moment arm, and stiffness of the muscles significantly increased the bending stiffness.

Similarly, the first 15 g frontal impact pediatric biofidelity response corridors (Figures 12 and 13) were created for future pediatric ATD neck design specifications from uncertainty analysis of the models in this loading scenario. Uncertainty analysis demonstrated that the z-direction vertebral geometry scale factor had the largest effect on the pediatric kinematic translation response, as increasing this value increased the length of the pediatric neck. As can be expected because of their smaller neck length, the heads of the pediatric models translated less than the adult. Peak x-direction CG translations were 70% and 86% of the adult peak translations, which were essentially the same percentage as the vertebral z-direction scale factors used to create the six and ten year old models, respectively. For the kinematic rotation response, the most significant parameter was muscle PCSA. Increasing this value decreased the peak head rotation, which is likely the result of an increased bending stiffness due to an increased muscle PCSA. As the ratio of head MOI to head mass is very similar for the two pediatric models, they experienced very similar flexion rotations. Additionally, since this ratio was larger in the pediatric models than in the adult, the pediatric model heads experienced more flexion rotation than the adult, each rotating 11% more than the adult.

Both the pediatric six and ten year old models had higher head translational and rotational head accelerations than the adult, with the six year old having the highest accelerations. This can be explained by a simple mass spring on a moving base

model. Increasing the spring stiffness of the mass-spring model decreases the acceleration of the mass. This was demonstrated during the uncertainty analysis in which increasing the muscle PCSA, which increased the neck bending stiffness, significantly decreased head accelerations. This is important as higher pediatric head accelerations could lead to pediatric head injuries that would not have caused adult injury under identical loading scenarios. However, further work needs to be done to understand pediatric accelerational head injuries to fully study this possibility. Currently, the Head Injury Criterion (HIC) threshold for the six year old is the same as the adult (Eppinger et al. 1999).

Notably, in all models (pediatric and adult), the neck muscle protected the osteoligamentous spine by bearing a large portion of the cross-sectional neck loads during 15 g frontal impacts (Figure 11). At peak neck flexion, the overall neck was loaded in tension. However, at this point the osteoligamentous cervical spine was loaded in compression due to the tension in the muscles. Additionally, nearly all of the moment experienced by the total neck in 15 g frontal impacts was carried by the muscles. As a result, the moments experienced by the osteoligamentous spine were small, indicating that in frontal impacts the osteoligamentous spine is unlikely to fail in this mode. In fact, the high compressive loads experienced by the osteoligamentous spine suggest that the primary mode of neck failure in frontal impacts is compression.

Finally, this study is not without limitation. For one, a limitation of the comparison of model responses during pendulum certification tests to the Mertz corridors was that head and chest interactions were not modeled in the simulations. The Mertz corridors were created from cadaver frontal impact sled tests in which the OC moment was calculated from inverse dynamics of head accelerations and included “the summation of the moments of the neck and chin forces” (Mertz and Patrick 1971). Mertz and Patrick reported a volunteer static head flexion rotation limit of 66 degrees and a dynamic rotation limit of 70 degrees. The adult model surpassed these limits with a peak head rotation greater than 110 degrees, which would not have occurred with chin contact providing “a stop for forward head rotation” (Mertz and Patrick 1971). Another limitation of this study was that during the 15 g frontal impact simulation, the same T1 boundary conditions were applied to the pediatric models as those measured from adult volunteers. While doing this enables direct comparisons between adult and pediatric head and neck kinematics and kinetics, subjecting children and adults to the same

sled accelerations would likely result in different T1 accelerations, as demonstrated in low speed frontal sled tests (Arbogast et al. 2009). This study also removed the effects of muscle activation dynamics from the comparison by applying the same activation histories to the pediatric models as those of the adult model for 15 g frontal impacts.

CONCLUSION

Pediatric head and neck models were used to investigate the dynamic bending stiffness of the pediatric human neck during frontal impact induced via Hybrid III ATD neck certification pendulum loading. The neck response of both pediatric models (six and ten years old) was found to be qualitatively different from the pediatric HIII ATDs: the models demonstrated nonlinear softening behavior while the HIII ATDs experienced nonlinear stiffening. Additionally, the pediatric models’ response was less stiff than that of the pediatric HIII ATD: Specifically, the pediatric six and ten year old models were 53% and 67% less stiff than the HIII ATD, respectively. As a result, the models’ response was not predicted by the Irwin and Mertz (1997) scaled neck flexion corridors. Moreover, these validated pediatric models based on human pediatric biomechanical properties were used to create the first pendulum certification and 15 g frontal impact biofidelity corridors for future ATD design.

REFERENCES

- [1] Arbogast K, Balasubramanian S, Seacrist T, Maltese M, García-España J, Hopely T, Constans E, Lopez-Valdes F, Kent R, and Tanji H. 2009. “Comparison of kinematic responses of the head and spine for children and adults in low-speed frontal sled tests.” *Stapp Car Crash Journal* 53:329-372
- [2] Camacho DLA. 1998. “Dynamic Response of the Head and Cervical Spine to Near-vertex Head Impact: An Experimental and Computational Study.” Ph.D. Thesis, Department of Biomedical Engineering, Duke University, Durham, North Carolina
- [3] CDC. 2007. WISQARS (Web-based Injury Statistics Query and Reporting System) Centers for Disease Control and Prevention
- [4] Chancey VC. 2005. “Strength of the human neck: understanding the contributions of the ligamentous and muscular spine in tension and bending.” Ph.D. Thesis, Department of Biomedical Engineering, Duke University, Durham, North Carolina
- [5] Colebatch JG, Halmagyi GM, Skuse NF. 1994. “Myogenic potentials generated by a click-evoked vestibulocollic reflex.” *Journal of Neurology*,

- Neurosurgery, and Psychiatry 57:190-197
- [6] de Lange R, van der Made R, Feustel JR, Subbian T, and van Hoof J. 2001. "Development and evaluation of MADYMO child occupant dummy models." In Proceedings of the 4th North American MADYMO User's Meeting, pp. 1-13
- [7] Dejeannes M, Tarri C, Thomas C, and Kallieris D. 1984. "Exploration of Biomechanical Data Towards a Better Evaluation of Tolerance for Children Involved in Automotive Accidents." In Proceedings of the 28th Stapp Car Crash Conference, SAE 840530, pp. 427-440
- [8] Dibb AT. 2011. "Pediatric Head and Neck Dynamic Response: A Computational Study." Ph.D. Thesis, Department of Biomedical Engineering, Duke University, Durham, North Carolina
- [9] Dibb A, Cox C, Nightingale R, Jason L, Cutcliffe H, Myers B, Arbogast K, Searcrist T, and Bass C. 2013. "Importance of Muscle Activations for Biofidelic Pediatric Neck Response in Computational Models." Traffic Injury Prevention (in review)
- [10] Doherty B and Paver J. 1988. "Mathematical modeling of the hybrid III manikin head-neck structure." Mathematical and Computer Modelling 11:430-435
- [11] Dupuis R, Meyer F, Deck C, and Willinger R. 2006. "Three-year-old child neck finite element modelization." European Journal of Orthopaedic Surgery & Traumatology 16(3):193-202
- [12] Durbin DR, Chen I, Smith R, Elliott MR, and Winston FK. 2005. "Effects of Seating Position and Appropriate Restraint Use on the Risk of Injury to Children in Motor Vehicle Crashes." Pediatrics 115(3):305-309
- [13] Ewing CL and Thomas DJ. 1972. "Human head and neck response to impact acceleration, NAMRL monograph, 21". Naval Aerospace Medical Research Laboratory, Naval Aerospace Medical Institute, Naval Aerospace and Regional Medical Center, Pensacola, Fla
- [14] Federal Motor Vehicle Safety Standard - Part 572 - Subpart E - Hybrid III Test Dummy. Code of Federal Regulations, Title 49 - Transportation. 2011
- [15] Federal Motor Vehicle Safety Standard - Part 572 - Subpart N - Hybrid III Six-year-old Child Test Dummy. Code of Federal Regulations, Title 49 - Transportation. 2011
- [16] Foust DR, Chaffin DB, Snyder RG, Baum JK. 1973. "Cervical range of motion and dynamic response and strength of cervical muscles." In Proceedings of the 17th Stapp Car Crash Conference, SAE 730975, pp. 285-308
- [17] Hill AV. 1938. "The Heat of Shortening and the Dynamic Constants of Muscle. Proceedings of the Royal Society of London." Series B, Biological Sciences 126(843):136-195
- [18] Iman R, Campbell J, and Helton J. 1981a. "An approach to sensitivity analysis of computer models. Part I—Introduction, input, variable selection and preliminary variable assessment." Journal of Quality Technology 13(4):174-183
- [19] Iman R, Helton J, and Campbell J. 1981b. "An approach to sensitivity analysis of computer models: Part II—Ranking of input variables, response surface validation, distribution effect and technique synopsis." Journal of Quality Technology 13(4):232-240
- [20] Irwin A and Mertz HJ. 1997. "Biomechanical basis for the CRABI and Hybrid III child dummies." Technical Report, Society of Automotive Engineers SAE 973317
- [21] Kallieris D, Barz J, Schmidt G, Heess G, and Mattern R. 1976. "Comparison Between Child Cadavers and Child Dummy By Using Child Restraint Systems in Simulated Collisions." In Proceedings of the 20th Stapp Car Crash Conference, SAE 760815, pp. 513-542
- [22] Liu XJ and Yang JK. 2002. "Development of Child Pedestrian Mathematical Models and Evaluation with Accident Reconstruction." Traffic Injury Prevention 3(4):321-329
- [23] Loyd AM, Nightingale RW, Lee C, Bass CR, Frush D, Daniel C, Marcus J, Mukundan S, and Myers BS. 2010. "Pediatric Head Contours and Inertial Properties for ATD Design." Stapp Car Crash Journal 54:167-196
- [24] Luck, J.F., R.W. Nightingale, Y. Song, J.R. Kait, A.M. Loyd, B.S. Myers, and C.R. Bass. 2012. "Tensile failure properties of the perinatal, neonatal and pediatric cadaveric cervical spine." Spine [accepted – DOI: 10.1097/BRS.0b013e3182793873]
- [25] Luck JF, Nightingale RW, Loyd AM, Prange MT, Dibb AT, Song Y, Fronheiser L, and Myers BS. 2008. "Tensile mechanical properties of the perinatal and pediatric PMHS osteoligamentous cervical spine." Stapp Car Crash Journal 52:107-134
- [26] Marzougui D, Kan C, and Bedewi N. 1997. "Development and validation of an NCAP simulation using LS-DYNA3D." In Proceedings of the Fourth International LS-DYNA3D Conference, at Minneapolis, Minnesota, pp. 319-332
- [27] Medri M, Zhou Q, DiMasi F, and Bandak F. 2004. "Head-neck finite element model of the crash test dummy THOR." International Journal of Crashworthiness 9(2):175-186
- [28] Mertz H, Jarrett K, Moss S, Salloum M, and Zhao Y. 2001. "The Hybrid III 10-Year-Old Dummy." Stapp Car Crash Journal 45:319-328
- [29] Mertz HJ and Patrick LM. 1971. "Strength and Response of the Human Neck." In Proceedings of the 15th Stapp Car Crash Conference, SAE 710855, pp.

2903-2928

- [30] Meyer F, Roth S, and Willinger R. 2009. "Child neck FE model development and validation." *International Journal of Human Factors Modelling and Simulation* 1(2):244-257
- [31] Mizuno K, Iwata K, Deguchi T, Ikami T, and Kubota M. 2005. "Development of a three-year-old child FE model." *Traffic Injury Prevention* 6(4):361-371
- [32] Myers BS, Woolley CT, Garrett WE Jr., Slotter TL, Best TM. 1998. "The Influence of Strain Rate on the Passive and Stimulated Engineering Stress-Large Strain Constitutive Behavior of Skeletal Muscle." *J Biomechanical Engineering* 120(1):126-132
- [33] NHTSA. 1998. "Development and Evaluation of the Hybrid III type Six-Year-Old Child Dummy." Technical Report, Office of Crashworthiness Standards and Vehicle Research and Test Center: National Highway Traffic Safety Administration Docket Number 98-3972
- [34] Platzer P, Jaendl M, Thalhammer G, Dittrich S, Kutscha-Lissberg F, Vecsei V, and Gaebler C. 2007. "Cervical Spine Injuries in Pediatric Patients." *The Journal of Trauma* 62(2):389
- [35] Reid SE, Raviv G, Reid SE Jr. 1981. "Neck muscle resistance to head impact." *Aviation, Space, and Environmental Medicine*, pp. 78-84
- [36] Saul RA, Pritz HB, McFadden J, Backaitis SH, Hallenbeck H, and Rhule D. 1998. "Description and performance of the Hybrid III three-year-old, six-year-old and small female test dummies in restraint system and out-of-position air bag environments." In *Proceedings of the 16th International Technical Conference on the Enhanced Safety of Vehicles*, pp. 1513-1531
- [37] Schneider LW, Foust DR, Bowman BM, Snyder RG, Chaffin DB, Abdelnour TA, Baum JK. 1975. "Biomechanical properties of the human neck in lateral flexion." In *Proceedings of the 19th Stapp Car Crash Conference*, SAE 751156, pp. 455-485
- [38] Siegmund GP, Sanderson DJ, Myers BS, Inglis JT. 2003. "Awareness affects the response of human subjects exposed to a single whiplash-like perturbation." *Spine* 28(7):671-679
- [39] Tennyson SA, Mital NK, King AI. 1977. "Electromyographic signals of the spinal musculature during +Gz impact acceleration." *Orthopedic Clinics of North America* 8:97-119
- [40] Thunnissen J, Wismans J, Ewing CL, and Thomas DJ. 1995. "Human Volunteer Head-Neck Response in Frontal Flexion: A New Analysis." In *Proceedings of the 39th Stapp Car Crash Conference*, SAE 952721, pp. 439-460
- [41] Van Ee CA. 2000. "Tensile Properties of the Human Muscular and Ligamentous Cervical Spine." Ph.D. Thesis, Department of Biomedical

Engineering, Duke University, Durham, North Carolina

- [42] Winters JM. 1990. "Hill-based muscle models: a systems engineering perspective." In *Multiple muscle systems: biomechanics and movement organization*, edited by J. M. Winters, pp. 69-93. Springer-Verlag, New York City
- [43] Winters JM. 1995. "How detailed should muscle models be to understand multi-joint movement coordination?" *Human Movement Science* 14(4-5):401-442
- [44] Winters JM and Stark L. 1985. "Analysis of fundamental human movement patterns through the use of in-depth antagonistic muscle models." *IEEE transactions on biomedical engineering* 32(10):826-39
- [45] Winters JM and Stark L. 1988. "Estimated mechanical properties of synergistic muscles involved in movements of a variety of human joints." *Journal of Biomechanics* 21(12):1027-1041
- [46] Wismans J, Maltha J, Melvin JW, and Stalnaker RL. 1979. "Child Restraint Evaluation By Experimental and Mathematical Simulation." In *Proceedings of the 23rd Stapp Car Crash Conference*, SAE 791017, pp. 383-415
- [47] Wismans J, van Oorschot E, and Woltring JH. 1986. "Omni-Directional Human Head-Neck Response." In *Proceedings of the 30th Stapp Car Crash Conference*, SAE 861893, pp. 313-331
- [48] Yang K and Le J. 1992. "Finite element modeling of Hybrid III head-neck complex." In *Proceedings of the 36th Stapp Car Crash Conference*, SAE 922526, pp. 219-233